A 350 GHz high-resolution high-sensitivity passive video imaging system*

Daniel Becker[a], James Beall[a], Hsiao-Mei Cho[a], William Duncan[a†], Gene Hilton[a], Rob Horansky[a], Kent Irwin[a], Peter Lowell[a], Michael Niemack[a], Nick Paulter[a], Carl Reintsema[a], Frank Schima[a], Robert Schwall[a], Ki Won Yoon[a], Peter Ade[b], Carole Tucker[b], Simon Dicker[c], Mark Halpern[d]

[a]NIST-Boulder
[b]Cardiff University
[c]University of Pennslyvania
[d]University of British Columbia

ABSTRACT

We are developing a 350 GHz cryogenic passive video imaging system. This demonstration system uses 800 photon-noise-limited superconducting transition edge sensor bolometers. It will image a 1 m x 1 m area at a standoff distance of 16 m to a resolution of approximately 1 cm at video frame rates (20 frames per second). High spatial resolution is achieved by the use of an f/2.0 Cassegrain optical system with 1.3 m primary mirror. Preliminary testing of prototype detectors indicates that we can achieve a noise equivalent temperature difference (NETD) of 70 mK for the fully sampled 1 m x 1 m image at 20 frames per second.

1. INTRODUCTION

Millimeter-wavelength radiation penetrates clothing well and is non-ionizing, making it a good candidate for identifying threats held beneath clothing.[1] Active millimeter-wave systems have been deployed at airports and are commercially available, but require operation at close distances. For identifying threats at larger distances (more than eight meters), passive video imaging systems are available commercially[2] but have poor spatial and temperature resolution. Cryogenic passive imaging systems using superconducting transition edge sensors are also being developed. One system with 64 detectors produces video images with a noise equivalent temperature difference (NETD) of 0.5 K at 6 Hz with a resolution of 4 cm over a 2 m x 4 m area.[3–6] Another system has much lower noise on a per-detector basis, but currently has only 10 detectors.[7]

The millimeter and sub-millimeter astronomy community has spent the past several decades working on a very similar problem: high-speed mapping of high resolution images over a large field of view. A commonly used solution has been the use of large-format arrays of over 1000 superconducting transition edge sensor (TES) bolometers, with multiplexed readout using superconducting quantum interference devices (SQUIDs).[8–10] The development of this technology provides the opportunity to greatly increase temperature sensitivity of terrestrial passive imaging systems.

We are developing a cryogenic passive video imaging system for operation at distances of 16 m - 28 m. The focal plane will contain 800 photon-noise-limited TESs. The system is intended as a test-bed to explore trade-offs between NETD, resolution and video frame rate, with the goal of understanding what specifications are required to achieve the requirements of stand-off imaging applications.

The system will operate at a frequency of 350 GHz (850 μm) with 11 % fractional bandwidth. Spatial resolution will be 1 cm over a 1 m x 1 m field of view at distance of 16 m. We expect to generate video images at 20 frames per second. Measurements of prototype detectors indicate that the fully populated focal plane with 800 detectors should achieve NETD of 70 mK. In this paper we describe the optics, detectors, readout, cryogenics and current status of this system.

† Current Address: Intellectual Ventures, 11235 SE 6th St., Suite A 200, Bellevue, WA 98004
Send correspondence to Daniel Becker: E-mail: beckerd@boulder.nist.gov

Passive Millimeter-Wave Imaging Technology XIII, edited by David A. Wikner, Arttu R. Luukanen, Proc. of SPIE Vol. 7670, 76700M · © 2010 SPIE · CCC code: 0277-786X/10/$18 · doi: 10.1117/12.852932

2. DESIGN OVERVIEW

2.1 Optical Frequency Choice

The choice of frequency for a passive security imaging system is a tradeoff between the ability to penetrate clothing (favoring low frequencies) and spatial resolution (favoring high frequencies). The 3 dB point for attenuation through clothing ranges from 350 GHz - 1 THz (high frequencies for thin materials such as Nylon, lower for thicker materials such as wool).[11] We choose 350 GHz to keep clothing attenuation at or below 3 dB and provide good spatial resolution. 350 GHz is also the center of an atmospheric transmission band (see Figure 1).

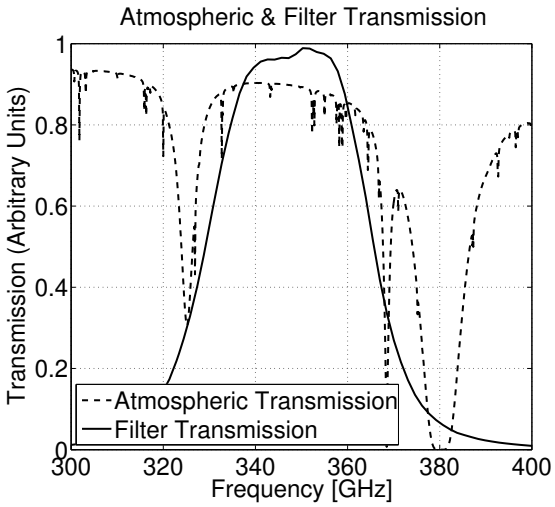

Figure 1. Plot showing measured transmission of our bandpass filter (solid lines) and typical atmospheric transmission (dashed lines). The passband is centered at approximately 350 GHz (850 μm) and has a full width at half-maximum of about 11 %.

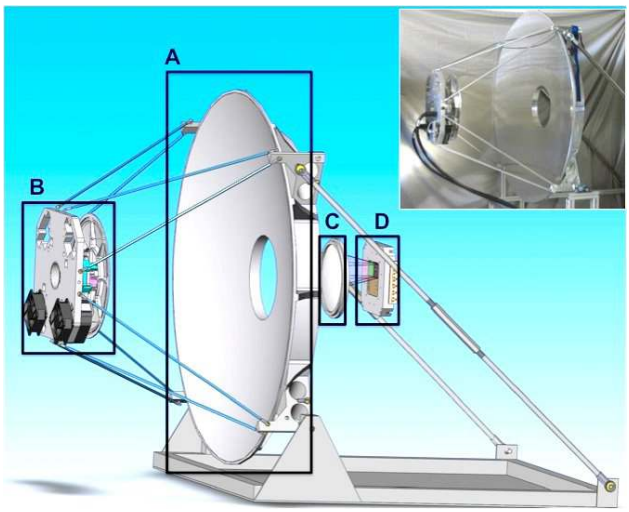

Figure 2. Schematic of optical system. Labels are (A) 1.3 m primary mirror, (B) secondary mirror with dithering mechanism, (C) cryostat window lens, (D) detector focal plane module, including bandpass filter. For clarity, the cryostat is not shown. Inset is a photograph of the primary and secondary mirror assembly.

2.2 Optics

Our optical system is an f/2.0 Cassegrain design. A 1.3 m elliptical primary mirror focuses light onto a hyperbolic secondary, which directs the light back through a central hole in the primary; the light then enters an ultra-high molecular weight (UHMW) polyethylene lens at the mouth of our cryostat. The lens makes the system telecentric, allowing use of a flat focal plane. The lens/cryostat combination can be moved relative to the primary mirror to focus the system at distances between 16 m and 28 m. The optics were simulated with ray-tracing software and shown to be diffraction-limited across the entire focal plane and at all focusing distances between 16 m and 28 m. See Figure 2 for an annotated picture of the optical system. A detailed description of the optics has been published elsewhere.[12]

The observation band is defined by a metal mesh filter[13] cooled to 850 mK, defining an optical bandwidth of 40 GHz (11 % FWHM fractional bandwidth); the measured passband of this filter is shown in Figure 1. Additional filters for thermal blocking are located at the 4 K, 50 K, and 300 K stages.[14] Total transmittance of the filter stack plus lens is expected to be 63 %.

At the focal plane, light is captured by smooth-walled conical feedhorns, which were chosen for their simplicity and ease of manufacture. To optimize coupling of the feedhorns to the rest of the optical system, we use feedhorns with a diameter of 3.2 mm, or approximately $2F\lambda$, where $F = 2.0$ is the f-number of the optics and $\lambda = 850$ μm is the optical wavelength. The taper half-angle is 9.4 deg, tapering to 0.6 mm circular waveguide that leads to the detectors. The feedhorn design was modeled with finite-element electromagnetic simulations, predicting a spillover efficiency of 68 %.

Because the point-spread-function of the optics has size $F\lambda$ on the focal plane, the feedhorns will be spaced farther apart than the Nyquist limit. Additionally, the feedhorns will cover only a portion of the diffraction-limited area of the focal plane. To generate fully sampled images, and to use the entire diffraction-limited extent of the optics, the secondary mirror will be moved by a set of actuators. This dithering of the secondary mirror will move the image across the focal plane, allowing fully sampled video images to be generated across the entire 1 m^2 target area.

To create a 1 m^2 image to resolution of 1 cm, 200^2 pixels per video frame are required. With an 800 detector system, this leads to a "dithering factor" of $200^2/800 = 50$, meaning that each detector will image 50 image pixels per video frame.

At the back of the 0.6 mm circular waveguide, in front of a quarter-wave backshort, the light is absorbed by a PdAu mesh patterned on a relieved membrane as described in section 2.4. Finite-element electromagnetic models indicate the PdAu mesh will absorb more than 90 % of the optical power coming down the waveguide. The mesh is sensitive to both polarizations.

2.3 Transition Edge Sensors

Optical power is detected by voltage-biased superconducting transition edge sensor (TES) bolometers.[15,16] Below a critical temperature T_c, a superconductor loses all resistance to DC electrical current (see Figure 3). The transition from the normal state to superconducting state is very sharp, allowing a superconductor that has been biased into the transition to serve as a very sensitive thermometer. Any signal that can be turned into a temperature change can then be detected as a change in the resistance of the superconductor.

Figure 4 schematically depicts the operation of a voltage-biased TES bolometer. Optical power is absorbed by an absorber that is thermally sunk to a superconducting film. Increasing optical power raises the temperature of the film, increasing the resistance of the TES, which decreases the current passing through it. This drop in current is detected by a SQUID. The device operates in a negative-feedback loop, with increasing optical power leading to lower V^2/R Joule heating, allowing the device to operate stably. While operating, the total power dissipated in the bolometer is a constant, P_{sat}, with any change in absorbed optical power compensated by an opposite change in Joule heating.

The absorber and film are connected to a low-temperature heat bath by a weak thermal link. The thermal conductance of this link determines the saturation power P_{sat} according to $P_{sat} = K(T_c^n - T_{bath}^n)$, where K and n depend on the geometry of the thermal link and the dominant heat transport mechanism in the temperature regime of interest; for our detectors we expect $n \approx 4.0$.[17] The differential thermal conductance G is then defined as $G = dP/dT_c = nKT_c^{n-1}$; G is an important parameter for the design of a bolometer.

The dominant source of intrinsic noise in our TES bolometers is thermal fluctuations of the temperature of the TES itself, due to random exchanges of energy between the TES and the low-temperature heat bath. This noise is given by $NEP_G = \sqrt{4k_B G T_c^2}$, where k_B is Boltzmann's constant.[17]

Photon noise is also a significant source of noise in our system. The expression for photon noise, including the effect of photon bunching, is given by[18]

$$NEP_{ph} = \sqrt{2h\nu P_{opt}(1 + \eta\bar{n})}, \tag{1}$$

where h is Planck's constant, ν is the central frequency, P_{opt} is the total optical loading, η is the optical efficiency (excluding feedhorn spillover efficiency, because the feedhorn spillover is terminated at 300 K), and $\bar{n} = [exp(h\nu/k_B T) - 1]^{-1}$ is the average photon occupation number per mode. For our system observing 300 K radiation, $\eta\bar{n} \approx 10$, so the bunching term is important. Total optical power per detector when observing a 300 K target will be $2\eta k_B T \Delta\nu = 190$ pW. Use of equation 1 then gives $NEP_{ph} = 1.0$ fW/$\sqrt{\text{Hz}}$.

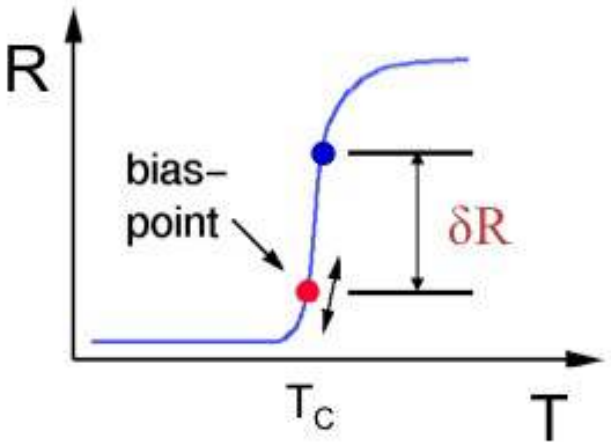

Figure 3. Illustrative plot of resistance vs temperature for a superconductor. The transition is typically very narrow, allowing the use of a superconductor as a sensitive thermometer. A TES detector is voltage-biased into the transition, with the bias point changing based on changes in optical power.

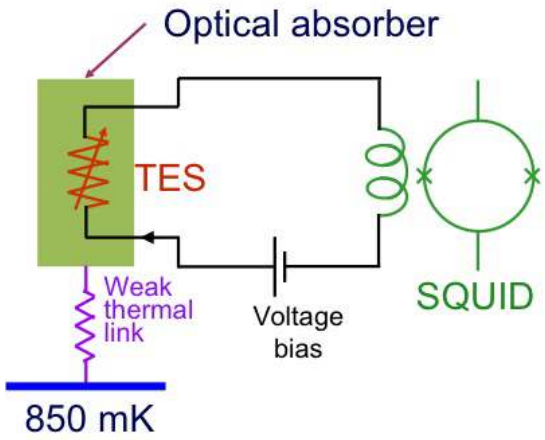

Figure 4. Schematic depiction of the operation of a TES. Optical power is absorbed onto the TES. Increases in absorbed optical power raises the temperature of the TES, raising its resistance. The dissipated V^2/R Joule power in the TES drops, compensating for the increase in optical power, leaving as constant the total dissipated power flowing out of the TES through the weak thermal link. This negative electro-thermal feedback allows the detector to operate stably. Changes in current passing through the TES are detected by a SQUID.

2.4 Design of Prototype Detectors

Figure 5 shows a picture of one of our prototype detectors. The device is fabricated on a relieved SiN membrane approximately 800 μm in diameter. Light is absorbed by a PdAu mesh, with dimensions (2 μm wide lines spaced 85 μm apart) chosen to match the wave impedance of the waveguide. The Al TES is located at the bottom center of the membrane, and has dimensions 63 μm x 63 μm. A 15 μm x 16 μm PdAu heater resistor is located near the center of the relieved membrane for use in testing.

We targeted our detectors to have $P_{sat} = 1$ nW (safety factor of 5). Given this saturation power, an aluminum TES with $T_c = 1.2$ K, a bath at 850 mK, and a target G of 4.5 nW/K should meet our NETD requirements. The dimensions of the eight SiN legs (11 μm wide x 40 μm long, 0.5 μm thick) were chosen to achieve this G.

This is a fairly large thermal conductance, which requires a large heat capacity C to keep the thermal time constant near the 1 ms that is optimal for our readout system. We have achieved this by adding a 2 μm thick gold ring around the outer diameter of the relieved membrane.

2.5 Readout

The array is read out by the SQUID-based time-division multiplexing (TDM) system developed at NIST.[19] This readout system has been in use for many years in a variety of applications, including millimeter-wave astronomy. The warm electronics will be provided by the Multi-Channel Electronics (MCE) system, which consists of a single crate that can read out all 800 of our detectors.[20] The combination of NIST SQUID TDM with the MCE is currently being used to collect data in the field at two different telescopes.[8,10] All hardware for the full 800 pixel array, including cryogenic wiring, is in place and installed in our cryostat.

2.6 Cryogenics

To cool our focal plane to an operating bath temperature of 850 mK, we use a two-stage refrigeration system. A commercially available cryogen-free Gifford-McMahon cryocooler allows us to reach 3 K. To cool the focal plane to below 1K we use a sealed ^{4}He sorption fridge. The sorption fridge is a custom-built system based on a design

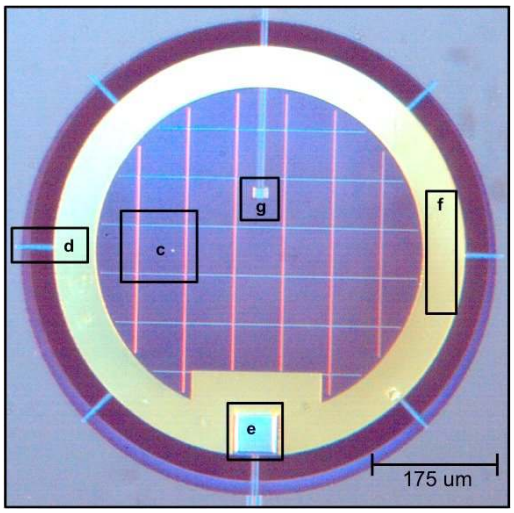

Figure 5. A picture of one of our fabricated TES detectors. The relieved area is 800 μm in diameter. The different components are: (c) PdAu absorbing mesh, lines 2 μm wide spaced 85 μm apart, (d) SiN legs connecting relieved membrane to the bulk Si substrate that serves as low-temperature bath, (e) thin-film Al TES, (f) Au ring providing sufficient heat capacity to slow down thermal response time of device for optimal readout (g) PdAu heater resistor used for testing.

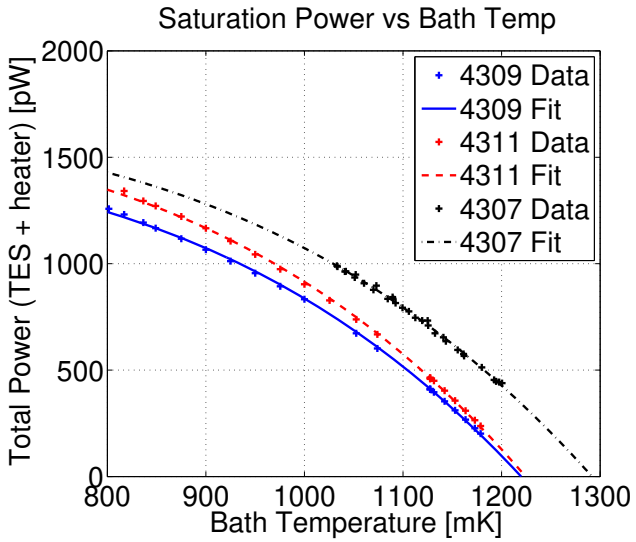

Figure 6. Plot showing saturation power P_{sat} vs bath temperature for three of our prototype devices. Fitting all three parameters n, K, and T_c implies $n \approx 3.6$. The fit to n is very weak, so for this paper we assuming $n = 4.0$ everywhere; this increases our estimated detector noise by a few percent. Detector 4307 was measured in a different cryostat with different thermometry, which could explain the temperature offset from detectors 4309 and 4311.

that has been proven in the field.[21] The system reaches a base temperature of 850 mK with a hold time of 36 hours under no optical load. Operation of this system will be fully automated.

3. CURRENT STATUS

We have fabricated and performed dark tests on prototype detectors. Our prototype devices have a transition temperature of approximately 1.23 K with a normal-state resistance of about 3.5 mΩ. Figure 6 shows measured saturation power vs. bath temperature for the three tested devices; the measured G values of 5.0 nW/K - 5.4 nW/K are about 10 % - 25 % higher than expected. These values of G imply NEP of 0.64 fW/$\sqrt{\text{Hz}}$ - 0.69 fW/$\sqrt{\text{Hz}}$.

Figure 7 shows the measured noise power spectral density for one of our detectors. The white noise level is about 0.8 fW/$\sqrt{\text{Hz}}$, 25 % higher than predicted based on G. Nevertheless our detectors are at the start of the photon-noise-limited level.

Adding the detector and expected photon noise in quadrature gives $NEP_{tot} = 1.3$ fW/$\sqrt{\text{Hz}}$. This total NEP can be converted to an NETD through the use of the radiometer equation,

$$NETD = \frac{NEP_{tot}}{2\sqrt{2\tau}k_B\Delta\nu\eta}, \tag{2}$$

where τ is the total integration time per pixel in the processed video frame, $\Delta\nu$ is the pre-detection optical bandwidth, and η is the total optical efficiency. For our system, $\tau = \frac{1}{50(20\text{ Hz})}$ (50 is the dithering factor defined in section 2.2), $\Delta\nu = 40$ GHz, and $\eta = 0.38$ (0.90 absorber efficiency, 0.63 filter stack efficiency, and 0.68 feedhorn spillover efficiency). Using equation 2, we estimate that our system will have $NETD = 70$ mK across the full field of view at 20 FPS.

Our next steps are to characterize our prototype detectors optically, generate still images with a 4-pixel prototyping setup, and then install the full 800-pixel focal plane.

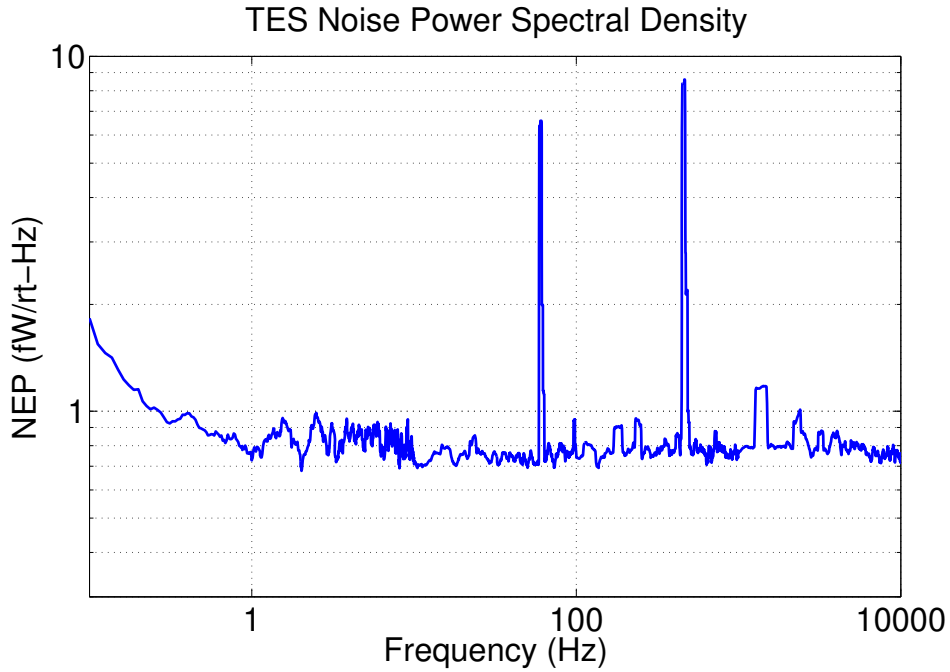

Figure 7. Plot showing measured noise equivalent power (NEP) spectral density for one of our detectors. The white noise level is about 0.8 fW/$\sqrt{\text{Hz}}$. The major peaks are at power line frequencies.

4. NEXT-GENERATION SYSTEM

The current system was designed for high sensitivity and low noise to facilitate the investigation of the tradeoffs inherent in an operational system. Adapting this system for field deployment will require reduction in cost, weight, and complexity. In addition to obvious modifications such as molded composite optical elements and simplified cryogenics, we are considering a readout system based on gigahertz micro-resonators that could be used to read out focal planes of either TESs or Microwave Kinetic Inductance Devices (MKIDs).[22] This readout system will read out hundreds of detectors with a single coaxial cable, greatly reducing the cost and complexity of cryogenic wiring, and allowing larger numbers of detectors to be placed on the focal plane.

5. CONCLUSION

We have designed a 350 GHz cryogenic terrestrial passive video imaging system by leveraging technology proven in the millimeter and sub-millimeter astronomy field. The video imager will use 800 TES bolometers to image a 1 m x 1 m field to a resolution of 1 cm at a distance of 16 m at video frame rates. Measurements of our prototype pixels indicate that they are close to being photon-noise-limited, and we should be able to achieve an NETD of 70 mK across the full field of view at 20 FPS. Our next steps are to generate still images with a four-pixel prototyping setup, followed by installation of the full 800-pixel focal plane.

REFERENCES

[1] R. Appleby, "Passive millimetre–wave imaging and how it differs from terahertz imaging," *Philosophical Transactions A* **362**(1815), p. 379, 2004.

[2] C. Mann, "First demonstration of a vehicle mounted 250GHz real time passive imager," in *Proceedings of SPIE*, **7311**, p. 73110Q, 2009.

[3] A. Luukanen and J. Pekola, "A superconducting antenna-coupled hot-spot microbolometer," *Applied Physics Letters* **82**, p. 3970, 2003.

[4] E. Grossman, C. Dietlein, J. Bjarnason, A. Luukanen, M. Leivo, and J. Pentilla, "THz microbolometers for imaging applications," in *Infrared, Millimeter and Terahertz Waves, 2008. IRMMW-THz 2008. 33rd International Conference on*, pp. 1–1, 2008.

[5] A. Luukanen, P. Helistö, P. Lappalainen, M. Leivo, A. Rautiainen, H. Toivanen, H. Seppä, Z. Taylor, C. Dietlein, and E. Grossman, "Stand-off passive THz imaging at 8-meter stand-off distance: results from a 64-channel real-time imager," in *Proceedings of SPIE*, **7309**, p. 73090F, 2009.

[6] A. R. Luukanen, L. Grnberg, M. Grnholm, P. Lappalainen, M. Leivo, E. N. Grossman, and C. R. Dietlein, "Real-time passive terahertz imaging system for standoff concealed weapons imaging," in *Proceedings of SPIE*, **7670**, pp. 7670–3, 2010.

[7] T. May, G. Zieger, S. Anders, V. Zakosarenko, H. Meyer, M. Schubert, M. Starkloff, M. Rößler, G. Thorwirth, and U. Krause, "Safe VISITOR: visible, infrared, and terahertz object recognition for security screening application," in *Proceedings of SPIE*, **7309**, p. 73090E, 2009.

[8] D. Swetz, P. Ade, C. Allen, M. Amiri, J. Appel, E. Battistelli, B. Burger, J. Chervenak, A. Dahlen, S. Das, *et al.*, "Instrument design and characterization of the millimeter Bolometer Array Camera on the Atacama Cosmology Telescope," in *Proceedings of SPIE*, **7020**, p. 702008, 2008.

[9] J. Ruhl, P. Ade, J. Carlstrom, H. Cho, T. Crawford, M. Dobbs, C. Greer, N. Halverson, W. Holzapfel, T. Lanting, *et al.*, "The south pole telescope," in *Proceedings of SPIE*, **5498**, pp. 11–29, 2004.

[10] W. Holland, W. Duncan, B. Kelly, K. Irwin, A. Walton, P. Ade, and E. Robson, "SCUBA-2: a large-format submillimeter camera on the James Clerk Maxwell Telescope," in *Proceedings of SPIE*, **4855**, p. 1, 2003.

[11] J. Bjarnason, T. Chan, A. Lee, M. Celis, and E. Brown, "Millimeter-wave, terahertz, and mid-infrared transmission through common clothing," *Applied Physics Letters* **85**(4), pp. 519–521, 2004.

[12] W. Duncan, R. Schwall, K. Irwin, J. Beall, C. Reintsema, W. Doriese, H. Cho, B. Estey, G. Chattopadhyay, P. Ade, *et al.*, "An Optical System for Body Imaging from a Distance Using Near-TeraHertz Frequencies," *Journal of Low Temperature Physics* **151**(3), pp. 777–783, 2008.

[13] P. Ade, G. Pisano, C. Tucker, and S. Weaver, "A review of metal mesh filters," in *Proceedings of SPIE*, **6275**, pp. 62750U–1, 2006.

[14] C. Tucker and P. Ade, "Thermal filtering for large aperture cryogenic detector arrays," in *Proceedings of SPIE*, **6275**, p. 62750T, 2006.

[15] K. Irwin, "An application of electrothermal feedback for high resolution cryogenic particle detection," *Applied Physics Letters* **66**, p. 1998, 1995.

[16] A. Lee, P. Richards, S. Nam, B. Cabrera, and K. Irwin, "A superconducting bolometer with strong electrothermal feedback," *Applied Physics Letters* **69**, p. 1801, 1996.

[17] K. D. Irwin and G. C. Hilton, *Cryogenic Particle Detection*, ch. Transition Edge Sensors, pp. 63–149. Springer-Verlag Berlin Heidelberg, 2005.

[18] J. Zmuidzinas, "Thermal noise and correlations in photon detection," *Applied optics* **42**(25), pp. 4989–5008, 2003.

[19] P. de Korte, J. Beyer, S. Deiker, G. Hilton, K. Irwin, M. MacIntosh, S. Nam, C. Reintsema, L. Vale, and M. Huber, "Time-division superconducting quantum interference device multiplexer for transition-edge sensors," *Review of Scientific Instruments* **74**, p. 3807, 2003.

[20] E. Battistelli, M. Amiri, B. Burger, M. Halpern, S. Knotek, M. Ellis, X. Gao, D. Kelly, M. Macintosh, K. Irwin, *et al.*, "Functional description of read-out electronics for time-domain multiplexed bolometers for millimeter and sub-millimeter astronomy," *Journal of Low Temperature Physics* **151**(3), pp. 908–914, 2008.

[21] M. Devlin, S. Dicker, J. Klein, and M. Supanich, "A high capacity completely closed-cycle 250 mK 3He refrigeration system based on a pulse tube cooler," *Cryogenics* **44**(9), pp. 611–616, 2004.

[22] B. Mazin, P. Day, K. Irwin, C. Reintsema, and J. Zmuidzinas, "Digital readouts for large microwave low-temperature detector arrays," *Nuclear Instruments and Methods in Physics Research Section A: Accelerators, Spectrometers, Detectors and Associated Equipment* **559**(2), pp. 799–801, 2006.